

Shell and ligand-dependent blinking of CdSe-based core/shell nanocrystals†

Bonghwan Chon,^a Sung Jun Lim,^a Wonjung Kim,^a Jongcheol Seo,^a Hyeonggon Kang,^b Taiha Joo,^a Jeeseong Hwang^b and Seung Koo Shin^{*a}

Received 26th November 2009, Accepted 6th May 2010

DOI: 10.1039/b924917f

Blinking of zinc blende CdSe-based core/shell nanocrystals is studied as a function of shell materials and surface ligands. CdSe/ZnS, CdSe/ZnSe/ZnS and CdSe/CdS/ZnS core/shell nanocrystals are prepared by colloidal synthesis and six monolayers of larger bandgap shell materials are grown over the CdSe core. Organic-soluble nanocrystals covered with stearate are made water-soluble by ligand exchange with 3-mercaptopropionic acid. The light-emitting states of nanocrystals are characterized by absorption and emission spectroscopy as well as photoluminescence lifetime measurements in solution. The blinking time trace is recorded for single nanocrystals on a glass coverslip. Both on- and off-time distributions are fitted to the power law. The power-law exponents vary, depending on shell materials and surface ligands. The off-time exponents for organic and water-soluble nanocrystals are measured in the range of 1.36–1.55 and 1.25–1.37, respectively, while their on-time exponents are spread in the range of 1.53–1.86 and 1.85–2.17, respectively. Water-soluble surface passivation with thiolate prolongs the dark period regardless of shell materials and core/shell structures. Of the core/shell structures, CdSe/CdS/ZnS exhibits the longest bright state. The on/off-time exponents are inversely correlated, although the successive on/off events are not individually correlated. A two competing charge-tunneling model is presented to describe the variation of on- and off-time exponents with shell materials and surface ligands.

Introduction

Of the II–VI compound semiconductor materials, CdSe-based nanocrystals have drawn much attention because they offer size-tunable emission in visible color with narrow bandwidth and high quantum efficiency.^{1–6} Their high photostability affords great promise for applications of single nanocrystals in lasers,¹ optoelectronic devices,^{2,3} and biological imaging.^{4–6} However, single fluorescent nanocrystals exhibit blinking where the fluorescence intensity intermittently flickers on and off.^{7–10} In biological imaging,^{4,5} the blinking limits real-time tracking of nanocrystals, while in flow cytometry⁶ it hinders quantitative counting of cells. To overcome these limitations and hindrances, we need a better understanding of blinking.

The blinking phenomena of fluorescent nanocrystals appear to follow a simple power law, $P(\tau) \propto \tau^{-\alpha}$, for both on- and off-time probability distributions.^{11–13} The same power law has previously been proposed in the anomalous diffusion

model presenting α between 1 and 2, which describes the hopping time distribution of charge carriers in amorphous materials, where there is a dispersion in the distances between trapping sites and a dispersion in the potential barriers between these sites.¹⁴ The power law holds over large timescales regardless of nanocrystal size,¹³ shape,^{15,16} lattice structure,¹⁷ shell composition^{13,15,18,19} and surface passivating ligand^{18–22} under various substrates,^{16,23,24} temperatures¹³ and laser fluences.^{15,16,25} A number of models have been proposed to explain this power-law behavior.^{8,10} Most of them consider blinking as random switching between the emitting (on) electron–hole pair state and the non-emitting (off) charge-separated state.⁸ The predicted power-law exponents, α_{on} and α_{off} , vary depending on how different models treat the separated charges. The primitive random-walk model assuming spatial diffusion of electron around the nanocrystal predicts a value of 1.5 for α_{off} .²⁶ Another random-walk tunneling model considering spectral diffusion in phase space also yields $\alpha_{\text{off}} = 1.5$.¹³ The trap model assuming electron tunneling from the conduction band to multiple traps around the nanocrystal results in α between 1 and 2 for both on- and off-times.^{24,27} Meanwhile, the fluctuating barrier charge-tunneling model involving a three-level system suggests different exponents for on versus off events.^{12,28} On the other hand, the fluctuating nonradiative recombination model involving a four-level system predicts a value of 1.5 for both α_{on} and α_{off} with exponential cutoff.²⁹ A diffusion-controlled electron transfer model predicts a change in both α_{on} and α_{off} from 1.5 at long times to 0.5 at short times.^{30,31} The Anderson localization model suggests

^a Bio-Nanotechnology Center, Department of Chemistry, Pohang University of Science and Technology, San31 Hyoja-dong Nam-gu, Pohang, Kyungbuk 790-784, Korea. E-mail: skshin@postech.ac.kr; Fax: +82 (0)54 279 3399; Tel: +82 (0)54 279 2123

^b National Institute of Standards and Technology, Physics Laboratory, Optical Technology Division, 100 Bureau Drive, Gaithersburg, MD 20899, USA. Fax: +1 301 975 4580; Tel: +1 307 975 6991

† Electronic supplementary information (ESI) available: Powder X-ray diffraction patterns, analysis of the length of on/off-time following the *N*th off/on period, and mean values of power law exponents. See DOI: 10.1039/b924917f

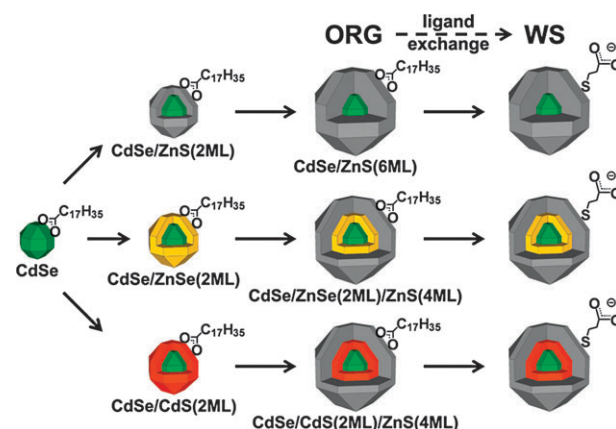
α_{on} between 0 and 2 and α_{off} between 1 and 2.³² These models mostly deal with electron diffusion, electron tunneling or electron transfer. However, our recent results suggest that single nanocrystals stay dark (off) more often as the number of surface hole-trap states increases, implying that in blinking dynamics hole traps on the surface of nanocrystal play a role as important as the electron trap.¹⁷

To further study the effect of surface trap states on the blinking phenomena, we have characterized the blinking of zinc-blende (ZB) CdSe-based type-I core/shell nanocrystals by varying shell materials and surface ligands. The cubic ZB lattice is considered better than the hexagonal wurtzite (W) lattice in examining the shell-dependent blinking because more uniform shell layers can be grown over the ZB lattice than the W lattice.³³ We have prepared three different core/shell nanocrystals starting from the same green-emitting CdSe core to have total six monolayers (MLs) of larger bandgap shell materials as shown in Scheme 1: CdSe/ZnS(6 ML), CdSe/ZnSe(2 ML)/ZnS(4 ML) and CdSe/CdS(2 ML)/ZnS(4 ML). In the core/double shell structure, either ZnSe(2 ML) or CdS(2 ML) are placed between the CdSe core and the outermost ZnS(4 ML) shell to successively reduce the lattice mismatch at the core/shell boundary, thus inducing less stacking faults than single shell CdSe/ZnS nanocrystals.³³ We have examined the lattice structure to check the epitaxial growth of shell and characterized optical properties of nanocrystals to define the bandgap structure of the bright state. The outermost ZnS shell allows the ligand exchange under identical conditions for all three core/shell nanocrystals. As-prepared nanocrystals are organic-soluble and they are made water-soluble by ligand exchange with 3-mercaptopropionic acid (MPA). Recently, we have shown that organic-soluble nanocrystals are primarily covered with stearate, while water-soluble ones are covered with thiolate through zinc–thiolate linkage.³⁴ Thus the three sets of organic- and water-soluble nanocrystals allow meaningful comparisons of the blinking statistics among well-characterized fluorescent nanocrystals as a function of shell materials and surface ligands. We have observed the blinking of nanocrystals on a clean glass coverslip with no polymers or additives.

Experimental

Preparation of zinc-blende CdSe/ZnS, CdSe/ZnSe/ZnS, CdSe/CdS/ZnS core/shell nanocrystals

Organic-soluble nanocrystals. Core/shell nanocrystals were prepared by layer-by-layer growth of shell materials over the same green-emitting CdSe core as previously described.³³ Briefly, ZB CdSe nanocrystals ($\lambda_{\text{em}} = 545 \text{ nm}$) were synthesized by reactions of cadmium stearate with selenium powder in 1-octadecene (ODE) at $\sim 240 \text{ }^\circ\text{C}$. About two MLs of ZnS, ZnSe, or CdS shells were grown over the CdSe core by reactions of shell precursors in ODE at $200\text{--}220 \text{ }^\circ\text{C}$ with 1-dodecylamine (DDA) as an additive. Zinc acetate, cadmium nitrate, bis(trimethylsilyl)sulfide, and bis(trimethylsilyl)selenide were used as precursors. About four MLs of the ZnS shell were grown over the core/shell nanocrystals to prepare CdSe/ZnS(6 ML), CdSe/ZnSe(2 ML)/ZnS(4 ML) and CdSe/CdS(2 ML)/ZnS(4 ML) core/shell nanocrystals. Nanocrystals



Scheme 1 Preparation of organic-soluble (ORG) CdSe/ZnS(6 ML), CdSe/ZnSe(2 ML)/ZnS(4 ML) and CdSe/CdS(2 ML)/ZnS(4 ML) nanocrystals covered with stearate ($\text{C}_{17}\text{H}_{35}\text{CO}_2^-$) and water-soluble (WS) counterparts carrying propionic acid thiolate.

were harvested, washed with methanol and acetone, dried under vacuum and stored in the dark. Resulting nanocrystals were soluble in chloroform and hexane, thus called *organic-soluble nanocrystals* (ORG-NCs).

Water-soluble nanocrystals. ORG-NC powder was dissolved in methanol containing MPA and tetramethyl ammonium hydroxide at $\sim 50 \text{ }^\circ\text{C}$. MPA-capped nanocrystals were precipitated, washed with ethyl acetate, harvested by centrifugation and dried under vacuum. Resulting nanocrystals were soluble in water, thus called *water-soluble nanocrystals* (WS-NCs).

Characterization of nanocrystals

X-Ray diffraction (XRD). Powder XRD patterns of nanocrystals were taken with a Rigaku SWXD diffractometer. XRD patterns are presented in Fig. S1 of ESI.†

Absorption and emission spectra. The absorption spectra were obtained with a UV/vis spectrometer (Agilent, 8453), and the emission spectra were taken with a fluorometer (PTI) at 1 nm resolution under 450 nm excitation. ORG- and WS-NC solutions ($\sim 1 \mu\text{M}$) were prepared in chloroform and water, respectively.

Photoluminescence decay of nanocrystals in solution. The photoluminescence (PL) decay was recorded using a time-correlated single-photon counting module (Becker & Hickl, SPC-630). The excitation light source was a 407 nm picosecond laser operating at the 2.5 MHz repetition rate (PicoQuant, LDH-P-C-405, pulse energy of 35 pJ). The laser beam was focused onto the sample in a 1 cm quartz cuvette and the emitted light was collected in the backscattering geometry and fed into an optical fiber after filtering off the excitation light. The fiber output was connected to either a spectrograph (Chromex, 250-IS 300 gr/mm) equipped with a liquid nitrogen-cooled charge-coupled device (CCD) (Princeton Instruments, LN/CCD-1024E) to take the dispersed PL spectra or a monochromator (Acton, SP-150 1200 gr/mm) equipped with a single-photon counting photomultiplier tube (Becker & Hickl,

PMC-100-1) to take the PL decay. The sample concentration was determined by band-edge absorbance: 0.18 μM for CdSe/ZnS, 0.23 μM for CdSe/ZnSe/ZnS, and 0.03 μM for CdSe/CdS/ZnS nanocrystals.

Single nanocrystal blinking measurements. ORG-NCs dissolved in chloroform or WS-NCs dissolved in water were dropped on a clean glass coverslip (Corning Inc., $\phi = 25$ mm, No 1.5). The coverslip was cleaned in a 1 M potassium hydroxide solution for 2 h, rinsed with ultrapure water (Barnstead, 18.2 M Ω), dried by nitrogen, and treated with a UV-Ozone cleaner (Jelight Company) for 40 min. The sample solution (~ 10 μL) was dropped on the coverslip and spin-coated (500 rpm for 5 s, 2000 rpm for 20 s). The coverslip was attached to a piezo stage (Mad City Labs, LP 100) and positioned above a 100 \times oil-immersion objective (Zeiss, N.A.1.45) mounted on an inverted fluorescence microscope (Zeiss, Axiovert 135). The sample was purged with argon to eliminate the effect of oxygen on blinking of nanocrystals. It was previously shown that oxygen in air induced blinking of nanocrystals embedded in a thin polymer film,³⁵ enhanced the fluorescence intensity from single nanocrystals placed in vacuum,³⁶ or mediated the blinking intensity level of single CdSe/CdS core/shell nanocrystals.³⁷ The 488 nm output from a cw solid state laser (Coherent, Sapphire 488-20) was focused onto a 50 μm pinhole for spatial filtering, expanded through a collimator, and passed through a bandpass filter to remove other spurious background emissions. The laser beam was reflected on a dichroic filter (Omega, 488 DRLP) and then focused onto the sample through the objective to form a spot ($1/e^2$ Gaussian radius of 0.22 μm) on the sample. The laser power incident on the dichroic mirror was 30 μW ^{21,38} and that on the sample was 10 μW . Thus, the laser fluence was below 5.7 kW cm⁻². The emission from the sample was collected by the same objective and divided by a 50/50 beam splitter (Newport, 10B20BS.1) to deliver either to an avalanche photodiode detector (Perkin-Elmer, APD SPCM-200-AQ) to take a fluorescence image and to trace blinking or to a CCD detector (Princeton Instruments, LN/CCD-1340EB) mounted on a monochromator (Action, SP-300) to take the PL spectra through a 488 nm notch filter (Kaiser) and a 750 nm shortpass filter (Semrock). A 128 \times 128 pixel image was obtained over a 10 \times 10 μm^2 area by rastering the sample for 1 ms at each pixel. A bright spot was repositioned at the center of the laser spot to monitor blinking from the single nanocrystal. A time trace of blinking was monitored for 6 min with 4 ms integration time. Single nanocrystal imaging and the data collection were processed with a scanning probe microscope controller (RHK Tech).

Results and discussion

Shell-dependent optical properties

The absorption and emission spectra of ORG-NCs dissolved in chloroform are shown in Fig. 1a. The epitaxial growth of shell shifts the emission maxima to the red from 545 nm for CdSe core nanocrystals to 556, 549 and 628 nm for CdSe/ZnS, CdSe/ZnSe/ZnS and CdSe/CdS/ZnS core/shell nanocrystals, respectively. The ZnS shell induces redshift of 11 nm and the

ZnSe/ZnS double shell leads to small redshift of 4 nm, whereas the CdS/ZnS double shell yields large redshift of 83 nm. These shell-to-shell variations of the spectral shift agree with our previous results obtained from CdSe/ZnS(4 ML), CdSe/ZnSe(2 ML)/ZnS(2 ML) and CdSe/CdS(2 ML)/ZnS(2 ML) nanocrystals.³³ We expect that both ZnS and ZnSe shells confine electron at the conduction band of the CdSe core, whereas the CdS shell expands the conduction band edge to the shell. Besides, ZB core/shell materials have the cubic lattice constant in a descending order of CdSe (6.05 \AA) > CdS (5.82 \AA) > ZnSe (5.67 \AA) > ZnS (5.41 \AA).³⁹ Thus the core/shell structures are under compressive strains due to the lattice mismatch between interfacing layers. The lattice mismatch at the interface is 10.6% in CdSe/ZnS, 6.3% in CdSe/ZnSe, 3.8% in CdSe/CdS, 4.6% in ZnSe/ZnS and 7.0% in CdS/ZnS. It seems that the outermost ZnS shell induces the redshift by exerting compressive strains to the inner lattice, the ZnSe shell relaxes such strains by acting as a buffer layer, and though the CdS shell also acts as a buffer layer it leads to the large redshift by lowering the conduction band edge.³³

The PL decay of ORG-NCs in chloroform is presented in Fig. 1b. The effective lifetime is 12.7 ± 0.02 , 11.8 ± 0.02 and 26.1 ± 0.02 ns for CdSe/ZnS, CdSe/ZnSe/ZnS and CdSe/CdS/ZnS, respectively. The PL lifetime of CdSe/CdS/ZnS is nearly twice those of other nanocrystals. The exponential fitting parameters, time constant and amplitude (in parenthesis), are as follows: [1.67 ± 0.01 ns (0.37), 19.0 ± 0.02 ns (0.63)] for CdSe/ZnS; [2.28 ± 0.01 ns (0.33), 16.5 ± 0.02 ns (0.67)] for CdSe/ZnSe/ZnS; [26.1 ± 0.02 ns (1.00)] for CdSe/CdS/ZnS. Addition of ZnSe(2 ML) inner shell slightly increases the fast time constant but decreases the slow time constant relative to the PL decay of CdSe/ZnS. On the other hand, addition of CdS(2 ML) inner shell removes the fast-decay component to make the PL decay nearly single-exponential, indicating that it helps circumvent initial fast nonradiative decay. The increase in ensemble PL lifetime means that the rate of transition from the radiative electron-hole pair state to the dark charge-separated state is reduced in single nanocrystals.

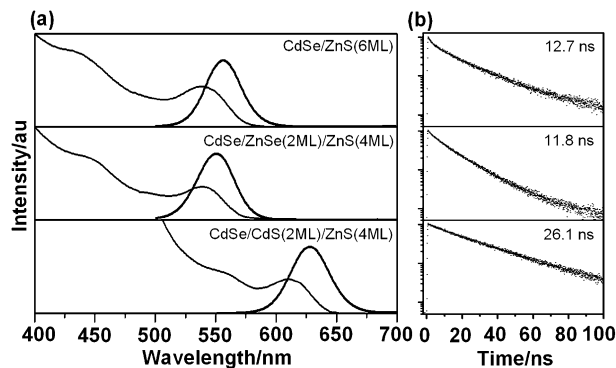


Fig. 1 (a) Absorption and emission spectra of organic-soluble nanocrystals dissolved in chloroform: λ_{em} (FWHM in nm) = 556 (35), 549 (35), and 628 (36) nm for CdSe/ZnS(6 ML), CdSe/ZnSe(2 ML)/ZnS(4p ML) and CdSe/CdS(2 ML)/ZnS(4 ML), respectively; (b) PL decay profiles and the effective lifetimes.

Shell-dependent blinking

The fluorescence image of ORG CdSe/CdS/ZnS single nanocrystals is presented in Fig. 2a as an example. There are typically less than ten single nanocrystals dispersed in an area of $10 \times 10 \mu\text{m}^2$. A single nanocrystal emits intermittently and shows bright and dark streaks along a scan direction. After confirming this trait of a single emitter, we move the sample stage to place the bright spot on the center of the gaussian laser beam for blinking and spectral measurements. The time-averaged PL spectra from each single nanocrystal are displayed in Fig. 2b. The emission spectra integrated for 5 s show spot-to-spot variations in emission maxima and widths: λ_{em} (FWHM in nm) = 617 (21), 631 (25), 624 (24), 629 (27) and 623 (25) nm for spots 1–5, respectively. When there are more than one resolvable peaks in the emission spectra, those spots are considered as nanocrystal aggregates and discarded from the pool of single nanocrystals. The average of five different spectra yields λ_{em} (FWHM in nm) of 628 (33) nm, which is nearly identical to those obtained from the solution ensemble spectra given in Fig. 1a.

The blinking time trace and histogram are presented in Fig. 3a and b for ORG- and WS-NCs, respectively. Of the ORG-NCs, CdSe/ZnS displays a bimodal on/off histogram. However, the average dark count is about the same as others.

In others, the time traces become spiky with significant intensity fluctuations, indicating that the on/off blinking cycle occurs more than once within a 4 ms bin.²¹ All WS-NCs show long tails in the on-state histograms. Apparently, the MPA conjugation on the ZnS shell reduces the fluorescence intensity and increases the blinking frequency. To see whether there is any correlation between the on and off events, we plotted the on-time duration following the N th off-event as well as the off-time duration following the N th on-event for ORG-NCs in Fig. S2 of the ESI.† We find no correlation between the two events.

To extract the probability distributions for both on- and off-times, we set the threshold separating “on” from “off” state at three times the standard deviation (3σ) of the average dark count.¹² The probability distributions are then fit to a power law of the form:¹³

$$P(\tau) = A\tau^{-\alpha}$$

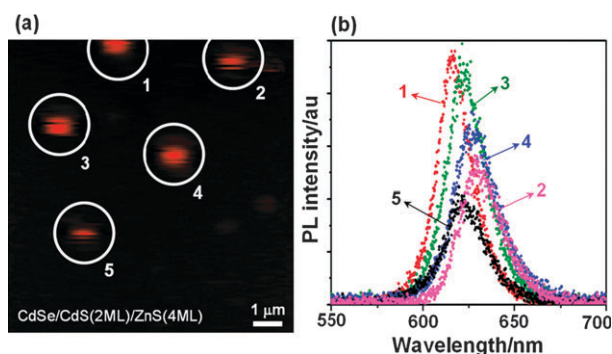


Fig. 2 (a) Fluorescence image of organic-soluble CdSe/CdS(2 ML)/ZnS (4 ML) single nanocrystals at 1 ms bin per pixel. The image size is $10 \times 10 \mu\text{m}^2$; (b) spot-to-spot variations of the emission spectra of single nanocrystals integrated for 5 s.

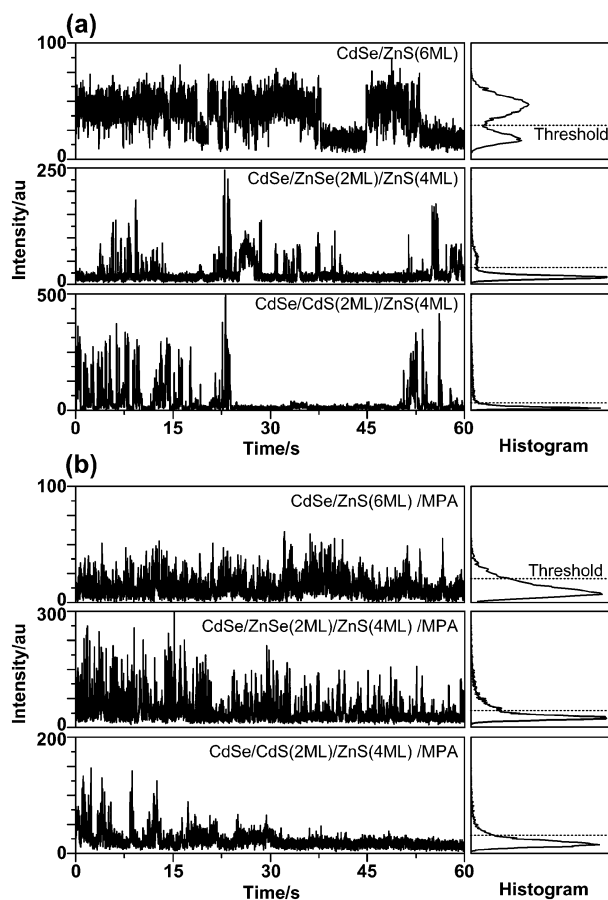


Fig. 3 Blinking time trace (left) and intensity histogram (right) of (a) organic-soluble (ORG) and (b) MPA-capped water-soluble (WS) CdSe/ZnS(6 ML), CdSe/ZnSe(2 ML)/ZnS(4 ML) and CdSe/CdS(2 ML)/ZnS(4 ML) nanocrystals. On/off threshold is marked by dotted line.

Although both on- and off-time exponents vary with threshold,⁴⁰ the power-law analysis suggests that the exponents derived from threshold of $3\text{--}6\sigma$ are comparable within errors (see Fig. S3 of the ESI.†).²¹ When the probability distributions are plotted on log-linear scales, a single exponential does not fit the data (see Fig. S4 and S5 of the ESI).

Both on- and off-time probability distributions for ORG- and WS-NCs are presented in Fig. 4a–d. In ORG-NCs, the on-time exponent α_{on} is spread in the range of 1.56–1.72, while the off-time exponent α_{off} is grouped around 1.35–1.61. In WS-NCs, α_{on} is scattered in the range of 1.57–2.39, while α_{off} is clustered around 1.30–1.37. Water-soluble MPA-conjugation significantly extends the off-times.

To get statistically more meaningful data, we examined a number of single nanocrystals: 12 CdSe/ZnS, 15 CdSe/ZnSe/ZnS and 33 CdSe/CdS/ZnS ORG-NCs; 12 CdSe/ZnS, 7 CdSe/ZnSe/ZnS and 15 CdSe/CdS/ZnS WS-NCs. For each sample, a 6 min long time trace is used to derive both on- and off-time exponents. Scattered values of (α_{on} , α_{off}) are plotted in Fig. 5a–c for CdSe/ZnS, CdSe/ZnSe/ZnS and CdSe/CdS/ZnS nanocrystals, respectively. The mean and error (95% confidence limit) of (α_{on} , α_{off}) are presented in Fig. 5d and listed in Table S1 in the ESI.† On average, the on-time

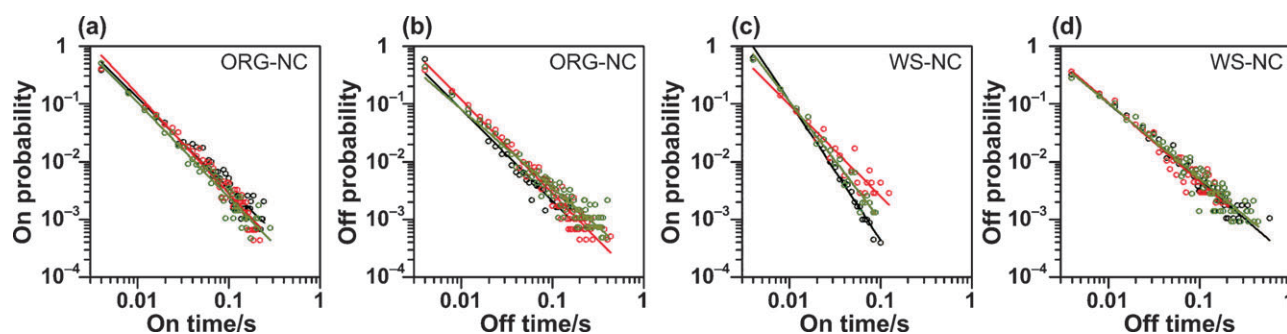


Fig. 4 On- and off-time probability distributions of organic-soluble (ORG) and water-soluble (WS) nanocrystals. For each nanocrystal, the whole 6 min time trace, a portion of which is shown in Fig. 3, is analyzed. (a) On-time and (b) off-time for ORG-NCs; (c) on-time and (d) off-time for WS-NCs. CdSe/ZnS(6 ML) in black, CdSe/ZnSe(2 ML)/ZnS(4 ML) in olive and CdSe/CdS(2 ML)/ZnS(4 ML) in red. The lines denote the least-squares fit to the power law. On- and off-time exponents (α_{on} , α_{off}) are $(1.56 \pm 0.03, 1.46 \pm 0.04)$, $(1.64 \pm 0.03, 1.35 \pm 0.02)$ and $(1.72 \pm 0.03, 1.61 \pm 0.03)$ for ORG CdSe/ZnS, CdSe/ZnSe/ZnS and CdSe/CdS/ZnS nanocrystal, respectively, and $(2.39 \pm 0.03, 1.32 \pm 0.02)$, $(2.05 \pm 0.05, 1.30 \pm 0.03)$ and $(1.57 \pm 0.05, 1.37 \pm 0.03)$ for WS CdSe/ZnS, CdSe/ZnSe/ZnS and CdSe/CdS/ZnS nanocrystal, respectively.

exponent α_{on} is spread in the range of 1.53–1.86 for ORG-NCs and 1.85–2.17 for WS-NCs, while the off-time exponent α_{off} is grouped around 1.36–1.55 for ORG-NCs and 1.25–1.37 for WS-NCs. The on-time exponent is more scattered than the off-time exponent in all cases.

Although each set of single nanocrystals yields widely scattered values of $(\alpha_{\text{on}}, \alpha_{\text{off}})$, some statistically meaningful trends appear when they are taken together: Obviously, α_{off} is scattered around 1.5. The MPA conjugation makes WS-NCs flicker more often (increased α_{on}) than ORG-NCs regardless of shell materials and core/shell structures. The off-time exponent decreases with increasing on-time exponent, suggesting that the on-time exponent is inversely correlated with the off-time exponent, although the successive on/off events are

not individually correlated. Of the three core/shell structures, CdSe/CdS/ZnS stands out as the least blinking structure: The CdSe/CdS/ZnS nanocrystal flickers much less (the least α_{on}) than the other two nanocrystals.

In comparison, the previously-reported values for power-law exponents are listed in Table S2 in the ESI.† Values are scattered around 1.5 from 1.29 to 1.79 for α_{off} and dispersed more widely from 1.42 to 2.29 for α_{on} ; α_{off} between 1.37 and 1.79 from ORG CdSe/ZnS nanocrystals on a glass slide;¹² α_{off} between 1.46 and 1.77 from ORG CdSe/ZnS nanocrystals embedded in a polymer film;²⁴ $(\alpha_{\text{on}}, \alpha_{\text{off}})$ of (1.61, 1.74) from ORG CdSe/ZnS nanocrystal on a fused silica coverslip;²⁸ $(\alpha_{\text{on}}, \alpha_{\text{off}})$ of (1.70, 1.29), (1.54, 1.35) and (1.42, 1.54) from ORG CdSe, ORG CdSe covered with octylamine and ORG CdSe/CdS nanocrystals dispersed in a polymer film, respectively;¹⁸ $(\alpha_{\text{on}}, \alpha_{\text{off}})$ of (1.71, 1.64) and (2.04, 1.57) from WS streptavidin-conjugated CdSe/ZnS nanoparticles in gel and on a glass slide, respectively;⁴¹ $(\alpha_{\text{on}}, \alpha_{\text{off}})$ of (1.73, 1.38), (2.29, 1.39), (2.27, 1.64) and (1.48, 1.64) from ORG bare CdSe/ZnS, WS carboxy-functionalized CdSe/ZnS, WS amine-functionalized CdSe/ZnS and WS mercaptoundecanoic acid-capped CdSe/ZnS nanocrystals on a glass slide, respectively;²¹ $(\alpha_{\text{on}}, \alpha_{\text{off}})$ of (1.71, 1.63), (2.16, 1.72) and (2.25, 1.66) from ORG CdSe/ZnS, WS CdSe/ZnS capped with aminoethanethiol and WS CdSe/ZnS capped with MPA dispersed in a polymer film, respectively.¹⁷ Apparently, the on-time exponent increases after water-soluble surface passivations.

To gain insights into the shell- and ligand-dependent blinking, we compared the band energy diagrams of three core/shell nanocrystals in Scheme 2. The size of ZB CdSe core is 1.35 nm in radius. The spacing of [111] ZB layer is 0.31, 0.33 and 0.35 nm for ZnS, ZnSe and CdS, respectively.³⁹ Thus, the nominal shell thickness is 1.86, 1.90 and 1.94 nm for CdSe/ZnS(6 ML), CdSe/ZnSe(2 ML)/ZnS(4 ML) and CdSe/CdS(2 ML)/ZnS(4 ML) nanocrystals, respectively. The bandgap of 2.23, 2.26 and 1.97 eV represents the emission maximum for each material displayed in Fig. 1. The band offset between the core and shell materials is taken from the literature.⁴² The tunneling barriers for electron and hole, ΔE_{e} and ΔE_{h} , should be greater than the bulk limit of 0.99 and 1.06 eV, respectively.⁴² In bulk CdSe, the exciton Bohr radius is 5.6 nm, which is the sum of 4.4 nm

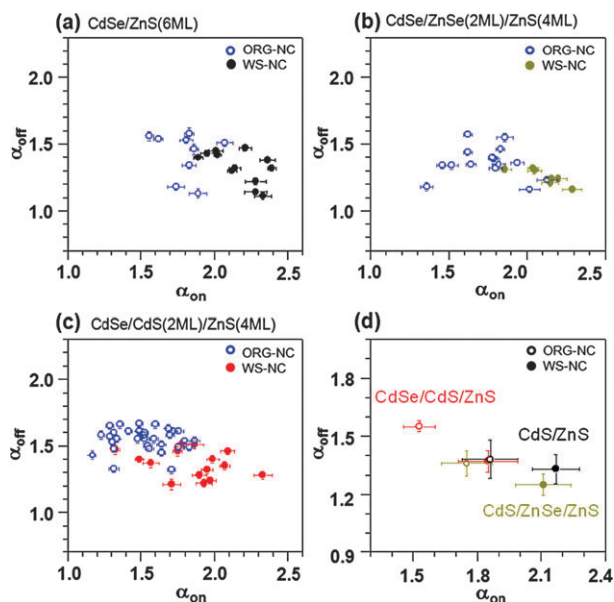
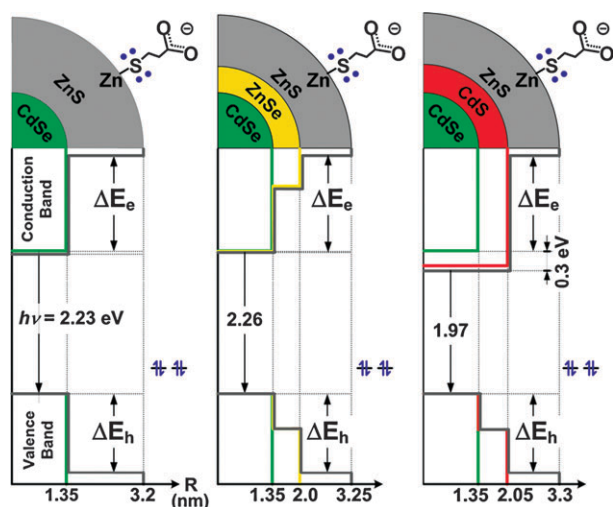


Fig. 5 Scatter plots of the power law exponents (α_{on} , α_{off}) from organic- (ORG) and water-soluble (WS) nanocrystals (NCs). (a) CdSe/ZnS(6 ML); (b) CdSe/ZnSe(2 ML)/ZnS(4 ML); (c) CdSe/CdS(2 ML)/ZnS(4 ML); (d) mean and error bound with a 95% confidence limit of the power-law exponents (α_{on} , α_{off}). ORG-NC is denoted by open circle and WS-NC by solid circle.



Scheme 2 Band energy diagrams of CdSe/ZnS(6 ML), CdSe/ZnSe(2 ML)/ZnS(4 ML) and CdSe/CdS(2 ML)/ZnS(4 ML) nanocrystals. The barrier for electron (ΔE_e) is greater than 0.99 eV and that for hole (ΔE_h) is greater than 1.06 eV. The bandgap (in eV) for each nanocrystal corresponds to the emission maxima given in Fig. 1. The zinc-thiolate linkage introduces two nonbonding electron pairs of sulfur as hole-trap states near the valence band edge.

for electron and 1.2 nm for hole.⁴³ Thus, electron is delocalized across the core/shell interface, while hole is localized at the CdSe core. Hence, the energy level of the conduction band more sensitively varies with shell materials than that of the valence band. The CdS/ZnS shell lowers the bandgap by 0.30 eV from 2.27 eV to 1.97 eV, whereas ZnS and ZnSe/ZnS shells lower it by only 0.04 and 0.01 eV, respectively. The lowering of bandgap by CdS/ZnS shell suggests the expansion of the conduction band edge, because the ZnSe/ZnS shell with the same valence band offset as the CdS/ZnS shell induces only 0.01 eV redshift. The expansion of conduction band to the CdS shell implies the reduction in shell thickness for electron tunneling (from 1.94 to 1.24 nm), but the lowering of bandgap indicates the elevation of barrier for electron tunneling by ~ 0.30 eV. Thus, CdSe/CdS/ZnS nanocrystals flicker less with extended on-time period than others because of the elevated tunneling barrier for electron.

It is also noteworthy that the surface conjugation with thiolate prolongs the off time period in all types of NCs. In contrast with ORG NCs, the thiolate in MPA-coated, WS NCs shortens on-time durations to nearly the same degree in all types of NCs, indicating that the effective tunneling barrier between the NC and the trap state are nearly identical regardless of the shell materials and core/shell structures. This implies that the extended off time is likely due to the thiol passivation by which hole trapping may also be induced. Two non bonding electron lonepairs in the sulfur atoms in the surface thiolate may serve as effective hole-trap states (Scheme 2).¹⁸ Once a hole is transferred to this trap state, a thick, 6 MLs of shell over the core could leave the NC in a charge-separated dark state for the extended off-time duration.

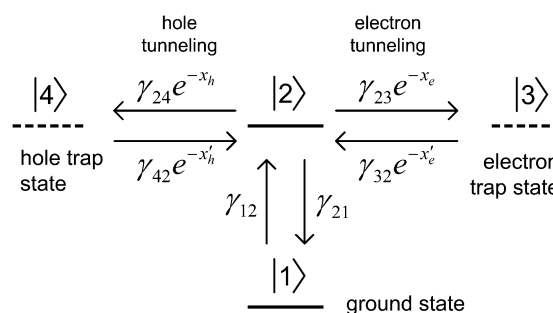
Recently, “giant” CdSe/CdS and CdSe/CdS/Cd_xZn_{1-x}S/ZnS nanocrystals dressed with 15–19 monolayers of shell^{44,45} have

been shown to blink much less than CdSe/ZnS nanocrystals emitting at the same wavelength. The Bohr exciton radius of electron is 4.4 nm in CdSe and 3.5 nm in CdS. In those giant nanocrystals with 5–7 nm thick shell, electron is delocalized over the expanded conduction band region with a small probability of tunneling beyond the surface boundary, whereas hole is confined at the CdSe core surrounded by 5–7 nm thick tunneling barrier. Thus both electron and hole tunneling seem to be greatly suppressed by thick shells. On the other hand, in the case of CdSe/ZnS nanocrystals, the significant lattice mismatch between the core and shell materials causes stacking faults and/or defects during the epitaxial growth of shell, which could act as interfacial trapping sites for blinking.

A two competing charge-tunneling model for blinking

To account for the shell- and ligand-dependent blinking of a single nanocrystal, we present a two-channel model that considers both electron- and hole-tunneling processes, as shown in Scheme 3. Kuno *et al.* have previously described a single charge-tunneling model,²⁸ based on a three-level system with a ground state |1⟩, radiating (neutral) state |2⟩, and nonradiating (ionized) state |3⟩. Blinking involves either electron or hole tunneling through the fluctuating barrier between the two states |2⟩ and |3⟩. In the single-channel model, absorption from |1⟩ to |2⟩ and emission from |2⟩ to |1⟩ occur with the rates of γ_{12} and γ_{21} , respectively. Ionization from |2⟩ to |3⟩ and neutralization from |3⟩ to |2⟩ occur with a range of rates that are exponentially distributed. The rates for switching-off and -on are $\gamma_{23} \exp(-x)$ and $\gamma_{32} \exp(-x')$, respectively. Stochastic variables x and x' are exponentially distributed by $L(x) = m \exp(-mx)$ and $L(x') = m' \exp(-m'x')$. Larger values of x and x' imply slower rates of tunneling.

We extend the single-channel model to explicitly include two competing channels to the dark state, one for electron tunneling and another for hole tunneling (Scheme 3). The off-time (τ_{off}) and on-time (τ_{on}) probability distributions [$P_e(\tau_{\text{off}})$ and $P_e(\tau_{\text{on}})$]



Scheme 3 Two competing charge-tunneling model for blinking. The ground state is denoted by |1⟩ and the light-emitting excited state by |2⟩. The rates of absorption and emission of light between |1⟩ and |2⟩ are γ_{12} and γ_{21} , respectively. Transitions to the charge-separated states, |3⟩ and |4⟩, by electron and hole tunneling, respectively, are modeled by exponentially-decaying rates for switching-off [$\gamma_{23} \exp(-x_e)$ for |2⟩ → |3⟩ and $\gamma_{24} \exp(-x_h)$ for |2⟩ → |4⟩] and switching-on [$\gamma_{32} \exp(-x'_e)$ for |3⟩ → |2⟩ and $\gamma_{42} \exp(-x'_h)$ for |4⟩ → |2⟩] processes. Stochastic variables x_i and x'_i ($i = e$ or h) are exponentially distributed, as given by $L(x_i) = m_i \exp(-m_i x_i)$ and $L(x'_i) = m'_i \exp(-m'_i x'_i)$.

for electron tunneling; $P_h(\tau_{\text{off}})$ and $P_h(\tau_{\text{on}})$ for hole tunneling] are expressed as eqn (1)–(4), respectively:

$$P_e(\tau_{\text{off}}) = \frac{m'_e \Gamma(1 + m'_e, \gamma_{32} \tau)}{\gamma_{32}^{m'_e}} \tau^{-(1+m'_e)}, \quad (1)$$

$$P_e(\tau_{\text{on}}) = \frac{m_e \Gamma(1 + m_e, \gamma_{23} \tau f)}{\gamma_{23}^{m_e}} \tau^{-(1+m_e)}, \quad (2)$$

$$P_h(\tau_{\text{off}}) = \frac{m'_h \Gamma(1 + m'_h, \gamma_{42} \tau)}{\gamma_{42}^{m'_h}} \tau^{-(1+m'_h)}, \quad (3)$$

$$P_h(\tau_{\text{on}}) = \frac{m_h \Gamma(1 + m_h, \gamma_{24} \tau f)}{\gamma_{24}^{m_h}} \tau^{-(1+m_h)}, \quad (4)$$

where Γ is an incomplete gamma function and $f = \gamma_{12}/(\gamma_{12} + \gamma_{21})$. When $\gamma_{23}\tau \gg 1$, $\gamma_{32}\tau \gg 1$, $\gamma_{24}\tau \gg 1$ and $\gamma_{42}\tau \gg 1$, the off- and on-time probability distributions follow the power law with exponents of $(1 + m'_e)$, $(1 + m_e)$, $(1 + m'_h)$ and $(1 + m_h)$, respectively.

The overall off-time probability distribution can be written as a linear combination of two off-events (eqn (5)), because the two switching-on processes ($|3\rangle \rightarrow |2\rangle$ and $|4\rangle \rightarrow |2\rangle$) are random and independent:

$$P(\tau_{\text{off}}) = c_e P_e(\tau_{\text{off}}) + c_h P_h(\tau_{\text{off}}) \propto \tau^{-\alpha_{\text{off}}}, \quad (5)$$

where $c_e + c_h = 1$. Thus, the off-time probability distribution with the two dark states runs between $P_e(\tau_{\text{off}})$ with the power-law exponent of $(1 + m'_e)$ and $P_h(\tau_{\text{off}})$ with the power-law exponent of $(1 + m'_h)$. On the other hand, the on-time probability distribution can not be expressed as a linear combination of the two on-time distributions because the two switching-off processes ($|2\rangle \rightarrow |3\rangle$ and $|2\rangle \rightarrow |4\rangle$) are competitive. The overall on-time probability distribution is written as eqn (6):

$$P(\tau_{\text{on}}) = \frac{m_e m_h G}{\gamma_{23}^{m_e} \gamma_{24}^{m_h} f^{1+m_e+m_h}} \tau^{-(1+m_e+m_h)}$$

$$G = \Gamma(1 + m_e, \gamma_{23} \tau f) \Gamma(m_h, \gamma_{24} \tau f) + \Gamma(m_e, \gamma_{23} \tau f) \Gamma(1 + m_h, \gamma_{24} \tau f) \quad (6)$$

When $\gamma_{23}\tau \gg 1$ and $\gamma_{24}\tau \gg 1$, G becomes constant and the on-time probability distribution follows the power law with an exponent of $(1 + m_e + m_h)$. As an example, the on- and off-time probability distributions calculated using eqn (5) and (6) are depicted in Fig. 6a and b, respectively. The trial values of $m_e = m'_e = 0.5$ and $m_h = m'_h = 0.2$ are assumed in order to approximately match with the experimental on-time exponents (α_{on}) of 1.7 ($1 + m_e + m_h$) and off-time (α_{off}) values in the range between 1.2 ($1 + m'_h$) and 1.5 ($1 + m'_e$). The trial values for γ and f are determined likewise. These theoretical predictions based on the hole-electron competing charge-tunneling model are qualitatively in line with experimental results. In brief, our theoretical model results in increased α_{on} and decreased α_{off} only when both electron and hole trap states exist, where the same results are observed when ORG-NCs are made water-soluble by thiolate surface conjugates regardless of shell materials and core/shell structures, as described above. Thus, both theory and experiments support the idea of having hole

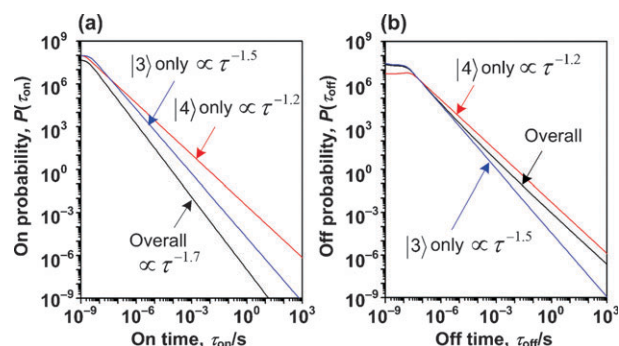


Fig. 6 Theoretical (a) on- and (b) off-time probability distribution assuming two different trap states, $|3\rangle$ and $|4\rangle$. Parameters used in calculations are $m_e = m'_e = 0.5$; $m_h = m'_h = 0.2$, $\gamma_{23} = 1 \times 10^9 \text{ s}^{-1}$, $\gamma_{24} = 2 \times 10^9 \text{ s}^{-1}$, $\gamma_{32} = 2 \times 10^8 \text{ s}^{-1}$, $\gamma_{42} = 1 \times 10^8 \text{ s}^{-1}$, $c_e = 0.83$ and $f = 0.86$.

tunneling induced by zinc-thiolate linkage in addition to electron tunneling. The two competing charge-tunneling model predicts that the two power-exponents need not be identical to each other.

The present model differs from others in several respects: (1) both electron- and hole-tunneling processes are explicitly considered; (2) both tunneling processes compete each other; (3) tunneling rates fluctuate with exponentially-distributed probabilities; (4) the time dependence is built-in on the stochastic tunneling or transition processes. In comparison, the multiple trap model²⁷ considers many electron traps near the nanocrystals with electron tunneling rates varying with distance and/or depth. The fluctuating nonradiative rate model²⁹ assumes the nonradiative relaxation of the hole-trap state to the ground state assisted by Auger-induced excitation. The more recent fluctuating nonradiative rate model⁴⁰ considers the nonradiative relaxation of the exciton through multiple recombination centers. In recent years, pulsed laser experiments showed the correlation of emission intensity, lifetime and polarization fluctuations in single nanocrystal blinking, suggesting time-dependent charge migration and fluctuation in nonradiative relaxation pathways.^{46–48} Although the present model properly describes the shell- and ligand-dependent exciton blinking of nanocrystals under cw laser irradiation, further study is underway to take those ultrafast phenomena involving biexciton⁴⁹ and trion^{37,50,51} into account.

Conclusion

Zinc-blende CdSe-based core/shell nanocrystals are prepared by epitaxial growth to have the six monolayers of larger bandgap materials over the green-emitting CdSe nanocrystals. Organic-soluble nanocrystals covered with stearate as well as water-soluble ones passivated with propionic acid thiolate are used to study blinking. The on-time exponents are more sensitive to both shell materials and surface ligands than the off-time exponents. Of the shell materials, CdS makes nanocrystals blink less than others. Between the two surface ligands, thiolate makes nanocrystals blink-off more. The two competing charge-tunneling model is proposed to explain experimental results. The electron- and hole-tunneling processes are separately considered as two independent random processes.

Under typical experimental conditions of μs to ms time scale, the overall off-time exponent lies between the two independent off-time exponents, whereas the overall on-time exponents is proportional to a sum of the two on-time exponents. Consequently, the on-time exponents vary more sensitively with shell materials and surface ligands than the off-time exponents. Most importantly, the apparent on- and off-time exponents need not to be universally identical to each other.

Acknowledgements

We thank support from Advanced Scientific Analysis Instruments Development Project administered by Korea Research Institute of Standards and Science, Nano Research and Development Program through the National Research Foundation funded by the Ministry of Education, Science, and Technology (Grant No. 2008-04540) of the Republic of Korea, and National Institute of Standards and Technology (NIST) Intramural Advanced Technology Program. Certain commercial equipment, instruments, or materials are identified in this paper to foster understanding. Such identification does not imply endorsement by NIST, nor does it imply that the materials or equipment identified are necessarily the best available.

References

- V. I. Klimov, A. A. Mikhailovsky, S. Xu, A. Malko, J. A. Hollingsworth, C. A. Leatherdale, H. J. Eisler and M. G. Bawendi, *Science*, 2000, **290**, 314–317.
- C. Wang, M. Shim and P. Guyot-Sionnest, *Science*, 2001, **291**, 2390–2392.
- A. L. Rogach, N. Gaponik, J. M. Lupton, C. Bertoni, D. E. Gallardo, S. Dunn, N. Li Pira, M. Paderi, P. Repetto, S. G. Ramanov, C. O'Dwyer, C. M. Sotomayor Torres and A. Eychmuller, *Angew. Chem., Int. Ed.*, 2008, **47**, 6538–6549.
- S. K. Shin, H.-J. Yoon, Y. J. Jung and J. W. Park, *Curr. Opin. Chem. Biol.*, 2006, **10**, 423–429.
- I. L. Medintz, H. T. Uyeda, E. R. Goldman and H. Mattoussi, *Nat. Mater.*, 2005, **4**, 435–446.
- P. K. Chattopadhyay, D. A. Price, T. F. Harper, M. R. Betts, J. Yu, E. Gostick, S. P. Perfetto, P. Goepfert, R. A. Koup, S. C. De Rosa, M. P. Bruchez and M. Roederer, *Nat. Med.*, 2006, **12**, 972–977.
- M. Nirmal, B. O. Dabbousi, M. G. Bawendi, J. J. Macklin, J. K. Trautman, T. D. Harris and L. E. Brus, *Nature*, 1996, **383**, 802–804.
- D. E. Gómez, M. Califano and P. Mulvaney, *Phys. Chem. Chem. Phys.*, 2006, **8**, 4989–5011.
- F. Cichos, C. von Borczyskowski and M. Orrit, *Curr. Opin. Colloid Interface Sci.*, 2007, **12**, 272–284.
- P. Frantsuzov, M. Kuno, B. Jankó and R. A. Marcus, *Nat. Phys.*, 2008, **4**, 519–522.
- M. Kuno, D. P. Fromm, H. F. Hamann, A. Gallagher and D. J. Nesbitt, *J. Chem. Phys.*, 2000, **112**, 3117–3120.
- M. Kuno, D. P. Fromm, H. F. Hamann, A. Gallagher and D. J. Nesbitt, *J. Chem. Phys.*, 2001, **115**, 1028–1040.
- J. P. Bouchaud and A. Georges, *Phys. Rep.*, 1990, **195**, 127–293.
- H. Scher and E. W. Montroll, *Phys. Rev. B: Solid State*, 1975, **12**, 2455.
- S. Wang, C. Querner, T. Emmons, M. Drndic and C. H. Crouch, *J. Phys. Chem. B*, 2006, **110**, 23221–23227.
- K. L. Knappenberger, Jr., D. B. Wong, W. Xu, A. M. Schwartzberg, A. Wolcott, J. Z. Zhang and S. R. Leone, *ACS Nano*, 2008, **2**, 2143–2153.
- Y. Kim, N. W. Song, H. Yu, D. W. Moon, S. J. Lim, W. Kim, H.-J. Yoon and S. K. Shin, *Phys. Chem. Chem. Phys.*, 2009, **11**, 3497–3502.
- D. E. Gómez, J. van Embden, J. Jasieniak, T. A. Smith and P. Mulvaney, *Small*, 2006, **2**, 204–208.
- C. D. Heyes, A. Y. Kobitski, V. V. Breus and G. U. Nienhaus, *Phys. Rev. B: Condens. Matter Mater. Phys.*, 2007, **75**, 125431.
- S. Hohng and T. Ha, *J. Am. Chem. Soc.*, 2004, **126**, 1324–1325.
- J. R. Krogmeier, H. Kang, M. L. Clarke, P. Yim and J. Hwang, *Opt. Commun.*, 2008, **281**, 1781–1788.
- V. Fomenko and D. J. Nesbitt, *Nano Lett.*, 2008, **8**, 287–293.
- K. T. Shimizu, W. K. Woo, B. R. Fisher, H. J. Eisler and M. G. Bawendi, *Phys. Rev. Lett.*, 2002, **89**, 117401.
- A. Issac, C. von Borczyskowski and F. Cichos, *Phys. Rev. B: Condens. Matter Mater. Phys.*, 2005, **71**, 161302(R).
- K. L. Knappenberger, Jr., D. B. Wong, Y. E. Romanyuk and Stephen R. Leone, *Nano Lett.*, 2007, **7**, 3869–3874.
- G. Margolin, V. Protasenko, M. Kuno and E. Barkai, *Adv. Chem. Phys.*, 2006, **133**, 327–356.
- R. Verberk, A. M. van Oijen and M. Orrit, *Phys. Rev. B: Condens. Matter Mater. Phys.*, 2002, **66**, 233202.
- M. Kuno, D. P. Fromm, S. T. Johnson, A. Gallagher and D. J. Nesbitt, *Phys. Rev. B: Condens. Matter Mater. Phys.*, 2003, **67**, 125304.
- P. A. Frantsuzov and R. A. Marcus, *Phys. Rev. B: Condens. Matter Mater. Phys.*, 2005, **72**, 155321.
- J. Tang and R. A. Marcus, *Phys. Rev. Lett.*, 2005, **95**, 107401.
- J. Tang and R. A. Marcus, *J. Chem. Phys.*, 2005, **123**, 204511.
- X. Xia and R. J. Silbey, arXiv:cond-mat/0601092v4 [cond-mat.mes-hall], 2006.
- S. J. Lim, B. Chon, T. Joo and S. K. Shin, *J. Phys. Chem. C*, 2008, **112**, 1744–1747.
- H. Min, Y. Kim, H. Yu, D. W. Moon, S. J. Lim, H.-J. Yoon, T. G. Lee and S. K. Shin, *Chem.–Eur. J.*, 2008, **14**, 8461–8464.
- F. Koberling, A. Mews and T. Basché, *Adv. Mater.*, 2001, **13**, 672.
- A. Müller, J. M. Lupton, A. L. Rogach, J. Feldmann, D. V. Talapin and H. Weller, *Appl. Phys. Lett.*, 2004, **85**, 381.
- D. E. Gómez, J. van Embden, P. Mulvaney, M. J. Fernée and H. Rubinsztein-Dunlop, *ACS Nano*, 2009, **3**, 2281–2287.
- H. Kang, M. M. Maye, D. Nykypanchuk, M. Clarke, P. Yim, J. Krogmeier, K. Briggman, O. Gang and J. Hwang, *Proc. SPIE*, 2007, **6430**, 643024.
- Physics of Semiconductor Devices*, ed. S. Sze, J. Wiley & Sons, New York, 2nd edn, 1981, pp. 848–849.
- P. A. Frantsuzov, S. Volkán-Kacsó and B. Jankó, *Phys. Rev. Lett.*, 2009, **103**, 207402.
- J. Yao, D. R. Larson, H. D. Vishwasrao, W. R. Zipfel and W. W. Webb, *Proc. Natl. Acad. Sci. U. S. A.*, 2005, **102**, 14284–14289.
- Y.-H. Li, A. Walsh, S. Chen, W.-J. Yin, J.-H. Yang, J. Li, J. L. J. Da Silva, X. G. Gong and S.-H. Wei, *Appl. Phys. Lett.*, 2009, **94**, 212109.
- D. Norris and M. G. Bawendi, *Phys. Rev. B: Condens. Matter*, 1996, **53**, 16338–16346.
- B. Mahler, P. Spinicelli, S. Buil, X. Quelin, J.-P. Hermier and B. Dubertret, *Nat. Mater.*, 2008, **7**, 659–664.
- Y. Chen, J. Vela, H. Htoon, J. L. Casson, D. J. Werder, D. A. Bussian, V. I. Klimov and J. A. Hollingsworth, *J. Am. Chem. Soc.*, 2008, **130**, 5026–5027.
- B. R. Fisher, H.-J. Eisler, N. E. Stott and M. G. Bawendi, *J. Phys. Chem. B*, 2004, **108**, 143–148.
- K. Zhang, H. Chang, A. Fu, P. Alivisatos and H. Yang, *Nano Lett.*, 2006, **6**, 843–847.
- D. Montiel and H. Yang, *J. Phys. Chem. A*, 2008, **112**, 9352–9355.
- V. I. Klimov, *J. Phys. Chem. B*, 2000, **104**, 6112–6123.
- P. Spinicelli, S. Buil, X. Quelin, B. Mahler, B. Dubertret and J.-P. Hermier, *Phys. Rev. Lett.*, 2009, **102**, 136801.
- P. P. Jha and P. Guyot-Sionnest, *ACS Nano*, 2009, **3**, 1011–1015.